Communications in Physics, Vol. 34, No. 1 (2024), pp. 63-74
DOI: https://doi.org/10.15625/0868-3166/18800

Effect of Sintering Temperature and Dwell Time on Structural and Ferroelectric Properties of $NiTiO_3$-$CoFe_2O_4$ composite

Luong Huu Bac†, **Dang Duc Dung**, **Nguyen Hoang Thoan**, **Nguyen Hoang Tuan and Pham Van Thang**

School of Engineering Physics, Hanoi University of Science and Technology, 1 Dai Co Viet, 10000 Hanoi, Vietnam

E-mail: †bac.luonghuu@hust.edu.vn

Received 2 September 2023
Accepted for publication 28 November 2023
Published 5 February 2024

Abstract. *The $0.9NiTiO_3$-$0.1CoFe_2O_4$ ceramic was prepared using the sol-gel method. The structural and ferroelectric properties of the ceramic were investigated. The material's structure was analyzed through X-ray diffraction and scanning electron microscopy. The fabricated materials consist of $NiTiO_3$ with a rhombohedral phase structure and $CoFe_2O_4$ with a cubic structure. The effect of sintering temperature and dwell time on the phase, microstructure, and ferroelectric properties of the ceramics was examined. With increasing sintering temperature and dwell time, the density of the bulk sample improved. The material sample was sintered at 1200˚C for 10 h, resulting in large particle size (~6 μm), few pores, and high density of approximately 97.5%. The composite material exhibited ferroelectric properties, as evidenced by the characteristic hysteresis loop observed in ferroelectric materials. At sintering temperatures of 1000˚C and 1100˚C for 2 and 5 h, the sample displayed poor ferroelectric characteristics. However, when the sample was sintered at 1200˚C for 10 hours, a notable enhancement in ferroelectric properties was observed.*

Keywords: $NiTiO_3$; ferromagnetism; ferroelectric property; composite; sintering.
Classification numbers: 81.20.Ev; 77.84.Lf.

1. Introduction

In the field of advanced materials, the category of multiferroic materials has attracted significant attention for their remarkable ability to exhibit coexisting ferroelectric and magnetic orderings [1]. The coexistence of these distinct properties in a single material has opened up exciting

opportunities for innovative device design, spanning from information storage to sensing technologies. At the heart of harnessing the full potential of multiferroic materials lies the intricate relationship between their structural, magnetic, and ferroelectric properties. Notably, the sintering process, a critical fabrication step, plays an important role in tailoring these properties for specific applications [2]. Multiferroic materials, characterized by their dual ferroic behavior, present an intriguing avenue for cross-coupled functionality, wherein changes in one property can influence and manipulate another. Such a phenomenon holds promise for developing next-generation devices with enhanced capabilities, efficiency, and versatility. However, achieving optimal multiferroic performance necessitates a deep understanding of the factors that shape the material's characteristics, and the sintering process stands as a primary determinant. Sintering, as a thermal treatment that enables the consolidation of particles into a solid body, directly impacts the microstructure and macroscopic properties of multiferroic materials [3]. The sintering temperature and duration are key variables that influence phase transformations, grain growth, defect concentration, and ultimately, the magnetic and ferroelectric responses [4]. Tailoring these parameters offers a unique avenue to engineer multiferroic materials with tailored functionalities, meeting the specific demands of diverse technological applications [5, 6]. In recent times, there has been a significant focus on studying the impacts of sintering condition on the structural, magnetic, and ferroelectric attributes of multiferroic materials [7, 8]. Through a methodical exploration of these factors, researchers have unearthed complex interconnections and revealed the fundamental mechanisms that govern the material's responses.

$NiTiO_3$ (NTO) has drawn particular interest due to its intriguing optical, electrical, and magnetic characteristics. It functions as a semiconductor with a bandgap ranging between 2.2 eV and 2.8 eV [9], while exhibiting antiferromagnetic behavior with a Neel temperature approximately between -269°C and -251°C [10]. $NiTiO_3$ displays ferroelectric properties at room temperature [11–13]. Modifying the magnetic traits of $NiTiO_3$ ceramics has often been achieved through the introduction of transition metal dopants [14]. The incorporation of these dopants can induce ferromagnetic features by creating oxygen vacancies and/or magnetic elements [9]. Nevertheless, the magnetic properties of the doped $NiTiO_3$ samples were relatively small. Recently, numerous prior studies have investigated composite materials involving ferroelectric substances like $BiFeO_3$, $BaTiO_3$, $PbTiO_3$, and spinel-type ferrites such as $MnFe_2O_4$ and $CoFe_2O_4$ [15–17]. Composites of ferroelectric and ferromagnetic phase exhibited tuning dielectric, piezoelectric, and ferroelectric properties. There was a noteworthy augmentation in magnetic and magneto-electric traits [18]. Remarkably, the magneto-electric and magnetic characteristics of this material experienced a substantial enhancement.

This manuscript aims to investigate the effect of sintering conditions on the structural and ferroelectric properties of $NiTiO_3$-$CoFe_2O_4$ composite. Our investigation revealed that ferroelectric properties of composite depended on the amout of $CoFe_2O_4$ [19]. Increasing amount of $CoFe_2O_4$ over than 10% could cause in high conductivity and degraded the ferroelectric properties of composites. Therefore, the composites with 10% $CoFe_2O_4$ content were used to study the dependence of magnetic and ferroelectric properties on sintering time and temperature. The composite materials were synthesized by sol-gel method. Our findings show that sintering temperature and dwell time significantly influence on the microstructure and ferroelectric properties of ceramic.

2. Experiment

2.1. Materials

Monohydrate citric acid ($C_6H_8O_7{\cdot}H_2O$), Nickel (II) nitrate hexahydrate ($Ni(NO_3)_2{\cdot}6H_2O$), ferric (III) nitrate nonahydrate ($Fe(NO_3)_3{\cdot}9H_2O$), Cobalt (II) nitrate hexahydrate ($Co(NO_3)_2{\cdot}6H_2O$) were purchased from Guangdong Xilong, Chemical Co., Ltd, China and tetraisopropoxytitanium ($Ti[OCH(CH_3)]_4$) was purchased from Sigma Aldrich. All chemicals were used without further purification.

2.2. Sample preparation

Composite of $0.9NiTiO_3$-$0.1CoFe_2O_4$ was synthesized using a sol-gel technique and named as NTO-10CFO. To serve as both a solvent and a chelating agent, a citric acid solution was employed. Initially, citric acid was dissolved in distilled water to create a solution with a molar concentration of 1.5 M. Tetraisopropoxytitanium (TTIP) was then carefully introduced into the solution and vigorously stirred for approximately 1 h at 70˚C. Subsequently, nickel nitrate was incorporated into the solution, and the resulting mixture was stirred for another hour. Cobalt nitrate and iron nitrate were subsequently added, maintaining a Co:Fe ratio of 1:2. The solutions underwent continuous stirring at 70˚C until gel formation occurred.

The gel precursor was subjected to drying at 100˚C overnight to eliminate excess water, transforming it into a xerogel foam block. This xerogel underwent heating at 400˚C for 2 h, followed by annealing at 800˚C in an air environment for 3 h, with a heating rate of 10˚C/min. After cooling to room temperature, the xerogel was ground using an agate mortar to yield composite powders.

For the P-E loop measurement, composite powder was thoroughly mixed with 3 wt.% polyvinyl alcohol (PVA, 5%). The resulting mixture was then subjected to uniaxial pressing, forming discs with a diameter of 10 mm and a thickness of approximately 1 mm under a pressure of 150 MPa. These pressed pellets were subjected to sintering temperature of 1000˚, 1100˚C, 1200˚C, utilizing a heating and cooling rate of 5˚C/min in an air environment, for a duration of 2, 5 and 10 h within a programmed box furnace. After sintering, the sintered pellets were polished, cleaned and silver electrode was deposited on both sides of the pellet.

2.3. Characterization

X-ray diffraction (XRD) pattern was measured by an X-ray diffractometer (Philips- X'PertPro) using Cu K_α (λ = 1.54056 Å) radiation. Microstructure of the samples was observed by scanning electron microscopy (Tabletop Microscope HITACHI TM4000Plus) with acceleration voltage of 15 kV. The densities of all sintered samples were determined by Archimedes method. Ferroelectric hysteresis loops (*P–E*) were tested by a ferroelectric tester (Radiant Precision Premier II).

3. Results and Discussion

3.1. Structural analysis

Figure 1 demonstrates the XRD pattern of as-synthesized NTO–10CFO composites prepared by sol-gel method. All observed diffraction peaks at 2θ = 24.03˚, 33.16˚, 35.72˚, 40.76˚, 43.69˚, 49.54˚, 53.90˚, 57.35˚, 62.35˚ and 64.06˚, corresponds to the (hkl) lattice planes of (012),

(104), (110), (11$\bar{3}$), (202), (024), (116), (018), (124) and (300), respectively. They belongs to the rhombohedral structure with R$\bar{3}$ space group of $NiTiO_3$ structure. The observed peaks and corresponding planes are well matched with standard JCPDS 33-0960. It is noted that the expected diffraction peaks of $CoFe_2O_4$ in composite materials can be detected diffraction peaks at 2θ = 30.31, 37.32 which exhibits a cubic spinel crystal structure with Fd$\bar{3}$m space group (JCPDS card number 22-1086). The X-ray diffraction spectra of the synthesized powders indicated that mixed crystalline spinel–ilmenite phases have been formed without any trace of foreign phases. These results exhibite the successful formation of the NTO and CFO crystal phases in the composites and no prominent chemical reactions formed during the synthesis process which obtaine the individual separation of ferroelectric and ferromagnetic phases.

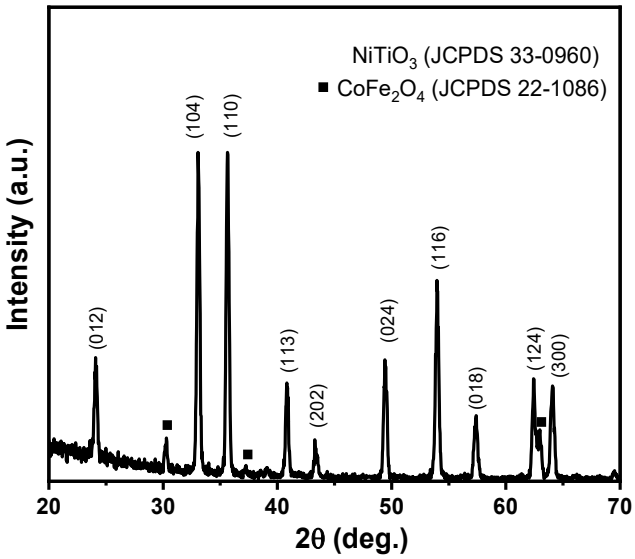

Fig. 1. XRD pattern of as-synthesized NTO–10CFO composites prepared by sol-gel method.

Figure 2 depicts the XRD patterns of the NTO–10CFO composites sintered at different temperatures for 5 h. Similar to the as-synthesized NTO–10CFO powder, the sintered bulk samples shows the all diffraction peaks matched with the two phases of $NiTiO_3$ and $CoFe_2O_4$. Increasing the sintering temperature leads to an increase in the intensity of the diffraction peaks and a narrowing of the diffraction peak without the addition of new diffraction peaks. This proves that increasing the sintering temperature does not change the phase structure of the material. Increasing sintering temperature can promote the diffusion of atoms between grain boundaries and increase the average grain size, which resulted in higher intensity and narrower peakwidth of XRD peaks. The initial stage of the diffusion process may involve the mixing of atoms right at the particle boundary. The process occurring at 1100˚C can lead to diffusion at the particle boundary, resulting in a disordered arrangement in the grain boundary layer. After sintering, the material still retains the single phase of ferroelectric and ferromagnetic phases.

Figure 3 illustrates the effect of surface morphology on the sintering temperature. The observed trend reveals an augmentation in sintered densities as the sintering temperatures rise.

This phenomenon can be attributed to the escalated reduction of porosity, facilitated by intensified diffusion at elevated temperature levels. The image clearly shows that the size of the grown particles is varied with sintering temperature. The grain size increases as the sintering temperature increases. With samples sintered at low temperature, the particle size is small. Many pores still existed on the surface and the grain size was non-uniform. As the sintering temperature increases, the grain size is significantly increased due to the diffusion of atoms across the grain boundary regions and fusion. The pores on the surface of the material are also gradually narrowed. At the sintering temperature of 1200˚C, the sintered sample has large particle size, uniform surface, and few pores.

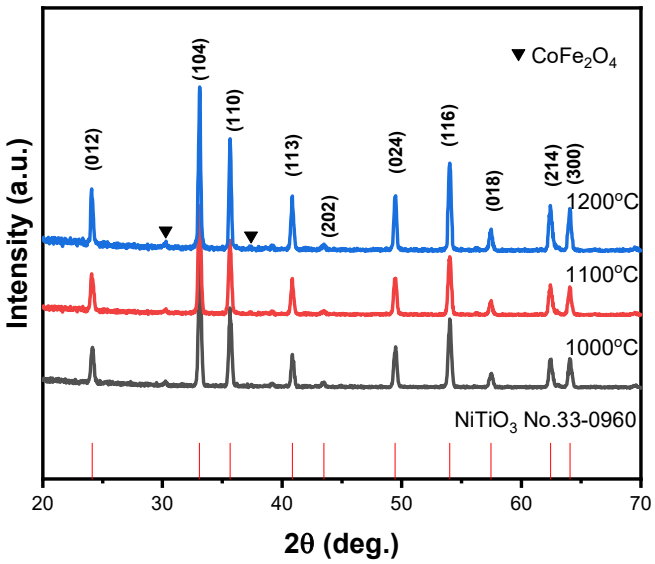

Fig. 2. XRD patterns of NTO–10CFO composite samples sintered at different temperatures.

Figure 4 demonstrates the true density and relative density of NTO-10CFO ceramics at different sintering temperatures. The sample sintered at temperature of 1200˚C shows the highest surface density and the pores almost disappeared. The sintered density increases from 92% at 1000˚C to 96% of the theoretical density at 1200˚C. The corresponding grain sizes increase from 0.7 μm at 1000˚C to 3.4 μm at 1200˚C. The ferroelectric characteristics are significantly influenced by the material's density and grain size. In the current investigation, the sintering temperature exhibits a substantial impact on the microstructure of the NTO-CTO ceramics. Chandrakala et al. has reported a similar sintering result when they researched on $0.5Ba(Zr_{0.2}Ti_{0.8})O_3$-$0.5(Ba_{0.7}Ca_{0.3})TiO_3$ ceramics. The sintered density increases from 66% at 1400˚C to 97% of the theoretical density at 1500˚C and the corresponding grain sizes increase from 1 μm at 1400˚C to 10 μm at 1500˚C [7]. Kwon et al. investigated the effect of sintering on the structure of the lead free $0.97(Bi_{0.5}Na_{0.5})TiO_3$–$0.03(Ba_{0.5}Sr_{0.5})TiO_3$ ceramics. The relative sintered density of ~98.1% of the theoretical density at sintering temperature of 1125˚C, and reached the highest value of 99.3% at 1200˚C [8].

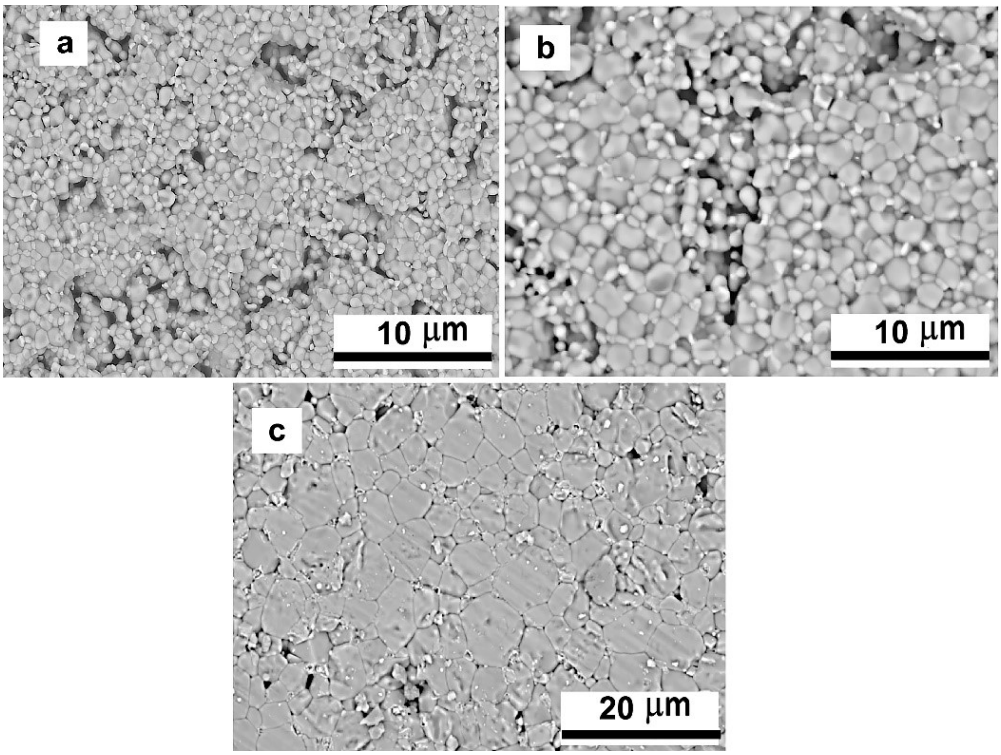

Fig. 3. SEM images of NTO-10CFO sintered at different temperatures a) 1000˚C, b) 1100˚C and c) 1200˚C for 5 h.

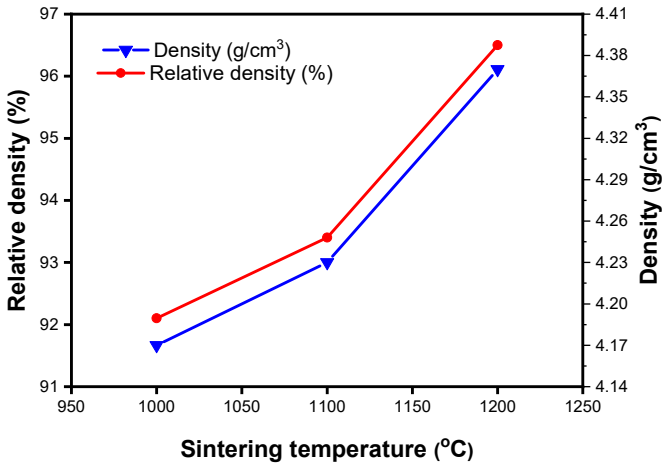

Fig. 4. True density and relative density of NTO-10CFO ceramics at different sintering temperatures.

The polarization-electric field (*P-E*) hysteresis loop of NTO–10CFO sintered at temperatures of 1000˚C, 1100˚C, 1200˚C at the same duration time of 5 h is shown in Fig. 5. Results show that when samples were sintered at temperature of 1000˚C and 1100˚C, residual polarization existed. However, the polarization decreases to near zero at a large applied-electric field. With this degeneracy loop, it is not possible to determine the saturation electrical polarization of the material samples. The reason for this decline can be explained by the low density and porosity of structure.

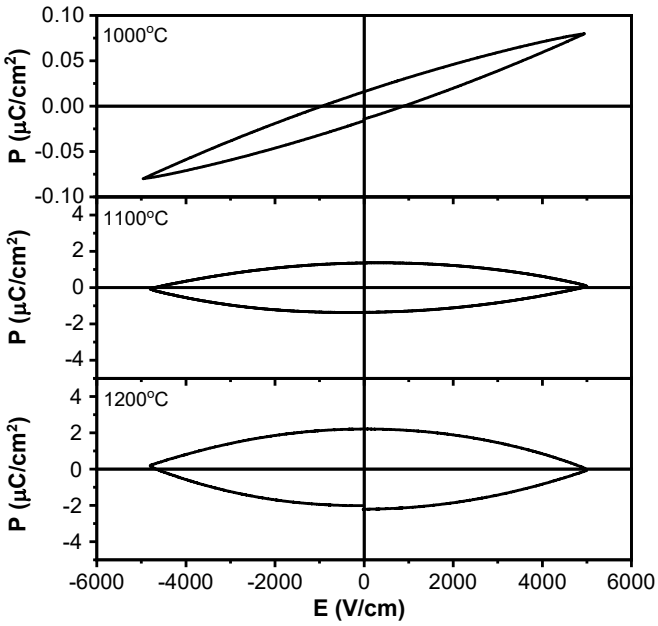

Fig. 5. Ferroelectric loops of NTO-10CFO composite sintered at different temperatures.

At these low sintering temperatures, the samples are in loose morphology with low density and high porosity. The particles are not sintered and connected together which give to high leakage current densities. However, well *P-E* hysteresis loop was obtained with sample sintered at 1200˚C with remanant polarization (P_r) value of 0.02 μC/cm^2 and maximum polarization (P_m) value of 0.08 μC/cm^2. The enhancement of ferroelectric properties with increasing sintering temperature has been reported in literature [4, 20]. This result can be explained by the decrease in the number of pores, the increase in grain size and in density of the material as the sintering temperature increases [21]. The well loop of sample sintered at 1200˚C exhibits the sintering temperature of this material. At this temperature, the diffusion of atom between two phases and particles result in the formation of dense morphology, which are favor of rising the polarization and reducing the leakage current density. In the next step, we keep the sintering temperature of 1200˚C and varied the dwell time from 2 h to 10 h to investigate the effect of dwell time on the structural and ferroelectric properties.

Figure 6 shows the X-ray diffraction spectrum of NTO–10CFO composite materials sintered at 1200˚C with different dwell time (2 h, 5 h and 10 h). From the diffraction results, it can be

seen that when the dwell time is increased, the phase structure of the material does not change. All diffraction peaks from XRD patterns coincide with the values in the JCPDS standard card number 033-0960 for $NiTiO_3$ phase and card number 22-1086 for $CoFe_2O_4$ phase. Regardless of the high sintering temperature and long dwell time up to 10 h, the secondary phases were not detected on all sintered samples which revealed the purity of the sintered sample.

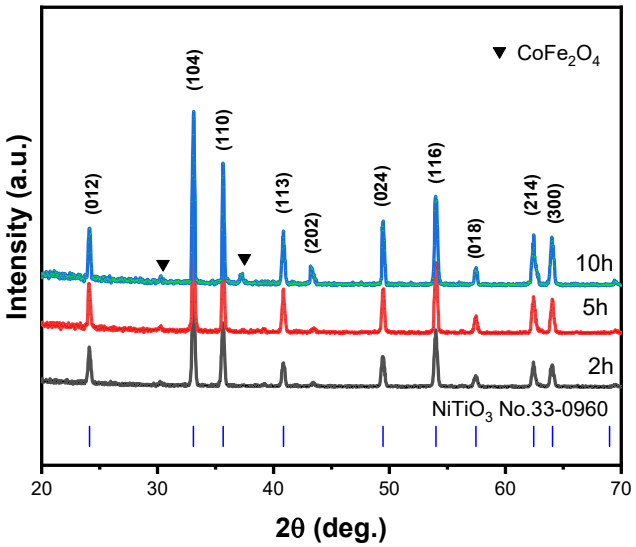

Fig. 6. XRD patterns of NTO-10CFO composite samples sintered at 1200˚C with different times.

Figure 7 shows SEM images of the composite samples sintered at 1200˚C with different dwell time Similarly with varying sintering temperature, prolonging dwell time is also in favor of the growth of grain and decrease of pores as the samples were sintered at 1200 ˚C . At the dwell time of 2 h, the particles have grown with a larger size and a more uniform surface, the pores are also smaller than that of the material fired for 5 h at 1000˚C and 1100˚C. However, at the dwell time of 2 h, the grain boundaries are still unclear and many voids on the surface which reveals the poor sintering ability. When the dwell time was up to 5 h, the grain boundaries became clearer and sharper. There are some small pores disappearingduring this dwell time. From image, it is evident that sample sintered at 5 h consisted both large and small grain with intergranular pores and densification was accompanied by intergranular neck growth by diffusion. When the dwell time is up to 10 h, the image appears in its end stage of sintering with all large grain size and clear grain boundaries with interconnectedangle. The sample sintered at temperature of 1200˚C shows the large grain size and high density. The average grain size increases from 3 μm for dwell time of 2 h to 6 μm for dwell time of 10 h. Figure 8 shows the true density and relative density of NTO-10CFO at different dwell time. The density increases from 95.6% to 97.4% of the theoretical density for dwell time increasing from 2 h to 10 h. This is consistent with the universal rule that long dwell time promotes the growth of grains in ceramic materials.

The polarization-electric field (*P-E*) hysteresis loop of NTO–10CFO sintered at 1200˚C for different time (2 h, 5 h and 10 h) is shown in Fig. 9. It is shown that when dwell time is 2 h,

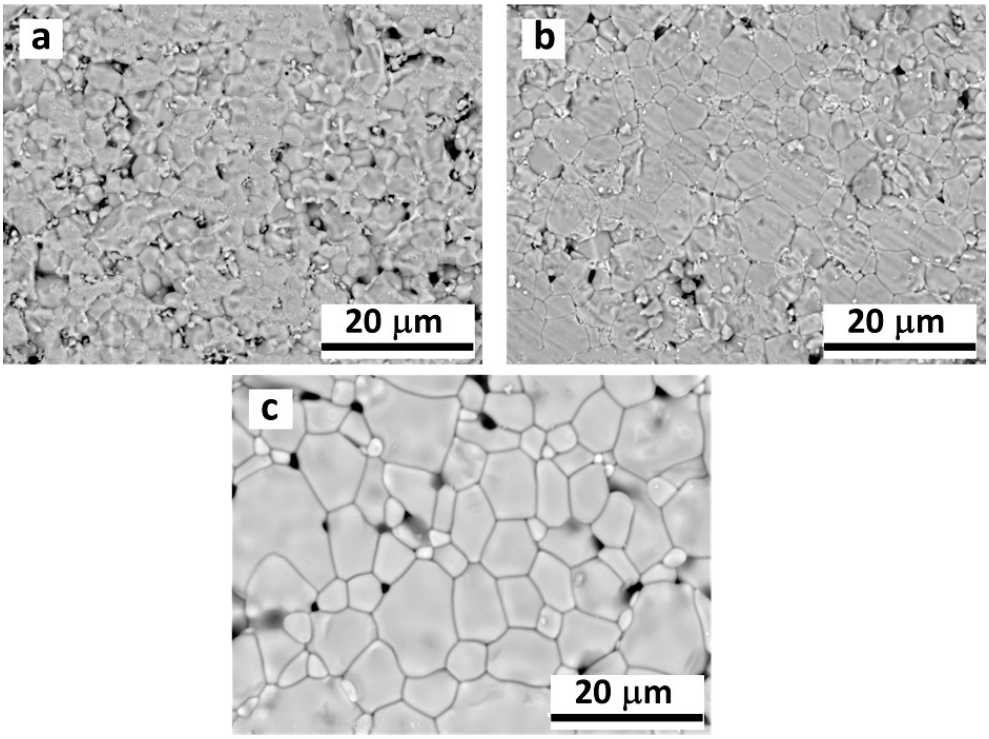

Fig. 7. SEM images of NTO-10CFO sintered at different dwell time a) 2 h, b) 5 h và c) 10 h.

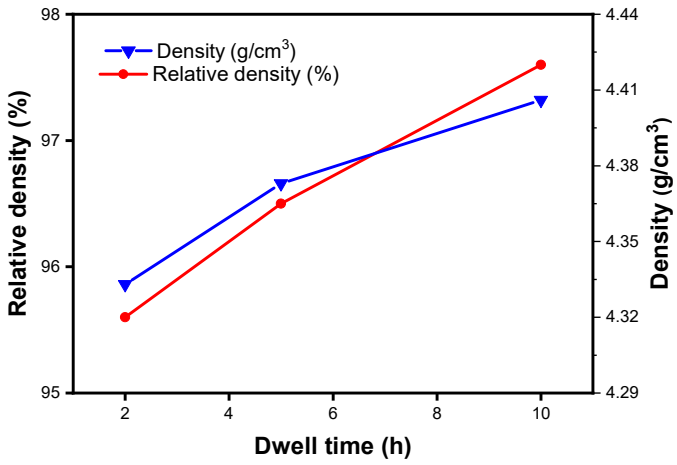

Fig. 8. True density and relative density of NTO-10CFO ceramics at different dwell time.

residual polarization has a large value of 0.65 μC/cm^2. However, the polarization is degraded at high applied electric field. The reason for this degradation is also explained via structure of

sintered properties. The low densification and high number of pores could caused in the poor ferroelectric property. As the dwell time is 5 h and 10 h, The *P-E* loops of prepared samples showed a typical *P-E* loop, indicating the ferroelectric properties of these samples. However, the remnant polarization, saturature polarization and coercive field are strongly influenced by dwell time. The slim *P-E* loop can be observed with 2 h sintering. As dwell time increases, the *P-E* loop becomes larger. The observed remnant polarization P_r increases from 0.02 to 0.07 μC/cm^2, saturation polarization increases from 0.08 to 0.12 μC/cm^2 and the coercive field E_c increases from 0.92 to 1.77 kV/cm with dwell time increasing from 5 h to 10 h. The ceramic with large grains (sintered for 10 h) has much stronger ferroelectricity than those with small grains (sintered for 5 h). Variation of both remnant polarization P_r and coercive field E_c depends dramatically on the grain size. This results are agreed with the report by Alkathy et al. for La and Na doped $BaTiO_3$ [21], by Cheng et al. for $0.98(K_{0.5}Na_{0.5})NbO_3$–$0.02LaFeO_3$ ceramics [22] and by Li et al. for the $BiFeO_3$–$BaTiO_3$–$Bi_{0.5}Na_{0.5}TiO_3$ lead-free ceramics [23] which implies the importance of the microstructure in tuning ferroelectric properties of ceramics.

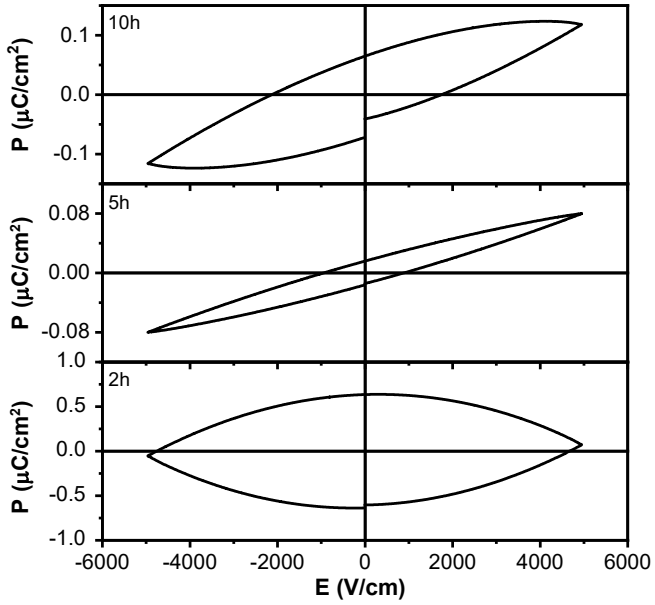

Fig. 9. Ferroelectric loops of NTO-10CFO composite sintered at different dwell time.

Figure 10 shows the variation of leakage current density (J) as a function of applied electric voltage (E) at room temperature for the NTO-10CFO sintered at 1200˚C at different dwell time. The J-E graphs are taken in both positive and negative voltage. It is observed from the graph that the value of leakage current decreases with an increase in dwell time. The smaller value of leakage current density is found for the ceramic sintered at 10 h. Smaller grain size and low density of sample sintered at 2 h which contributes to the increased leakage current density. In contrast, large grain size and high density of sample sintered at 10 h resulted in low leakage current density. The measured low leakage current densities for NTO-10CFO sintered at 10 h confirmed that the samples have high resistivity.

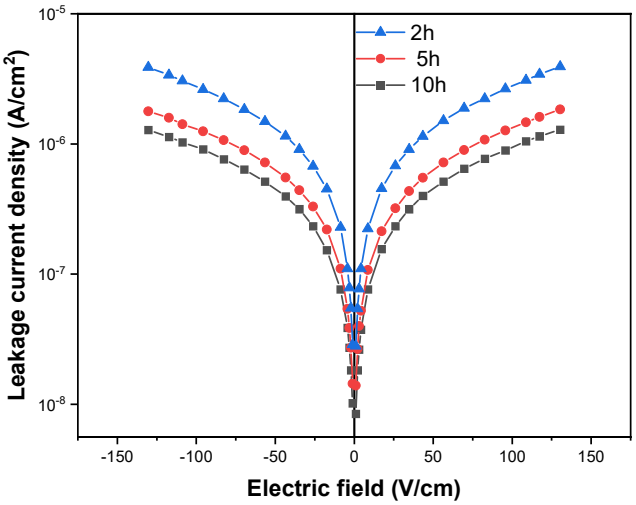

Fig. 10. Leakage current density plots for NTO-10CFO samples sintered at different dwell time.

4. Conclusion

The $0.90NiTiO_3$-$0.10CoFe_2O_4$ composite ceramic was prepared with different sintering temperature and dwell time to reveal the impact of the sintering conditions on structure and ferroelectric properties. All samples show two phases coexistence including of $NiTiO_3$ rhombohedral phase and $CoFe_2O_4$ cubic phase. The sintering temperature and dwell time does not affect on the phase structure. However, they significantly influence on the microstructure and ferroelectric properties. P-E loops confirm presence of ferroelectric ordering and remnant polarization as well as saturation polarization increases with increasing sintering temperature and dwell time. Large particle size and high density are achieved in the sintering temperature of 1200˚C and dwell time 10 h, which enhances ferroelectric properties. When the samples are sintered at 1200˚C, the relative density of the ceramics is 97.6%, average grain size is 6 μm and saturation polarization is 0.12 μC/cm^2.

Acknowledgment

This research is funded by Vietnam National Foundation for Science and Technology Development (NAFOSTED) under Grant number 103.02-2020.27.

References

[1] M.M. Vopson, *Fundamentals of multiferroic materials and their possible applications*, Crit. Rev. Solid State Mater. Sci. **40** (2015) 223.

[2] P. A. Jha, A.K. Jha, *Effect of sintering temperature on the grain growth and electrical properties of barium zirconate titanate ferroelectric ceramics*, J. Mater. Sci. Mater. Electron. **24** (2013) 1511.

[3] R. L. Coble, Sintering crystalline solids. I. intermediate and final state diffusion models, J. Appl. Phys. **32** (1961) 787.

[4] L. F. Zhu, B. P. Zhang, J. Q. Duan, B. W. Xun, N. Wang, Y.C. Tang and G.L. Zhao, *Enhanced piezoelectric and ferroelectric properties of $BiFeO_3$-$BaTiO_3$ lead-free ceramics by optimizing the sintering temperature and dwell time*, J. Eur. Ceram. Soc. 38 (2018) 3463.
[5] L. Liu, H. Fan, S. Ke and X. Chen, *Effect of sintering temperature on the structure and properties of cerium-doped 0.94(Bi0.5Na0.5)TiO_3-0.06$BaTiO_3$ piezoelectric ceramics*, J. Alloys Compd. **458** (2008) 504.
[6] C. Jiten, R. Gaur, R. Laishram, K.C. Singh, *Effect of sintering temperature on the microstructural, dielectric*, ferroelectric and piezoelectric properties of (Na0.5K0.5)NbO3 ceramics prepared from nanoscale powders, Ceram. Int. **42** (2016) 14135.
[7] E. Chandrakala, J. Paul Praveen, B.K. Hazra, D. Das, *Effect of sintering temperature on structural, dielectric, piezoelectric and ferroelectric properties of sol-gel derived BZT-BCT ceramics*, Ceram. Int. **42** (2016) 4964.
[8] Y.H. Kwon, G.H. Lee and J.H. Koh, *Effects of sintering temperature on the piezoelectric properties of (Bi,Na)TiO_3-based composites for energy harvesting applications*, Ceram. Int. **41** (2015) S792.
[9] M. A. Ruiz-Preciado, A. Kassiba, A. Gibaud and A. Morales-Acevedo, *Comparison of nickel titanate ($NiTiO_3$) powders synthesized by sol-gel and solid state reaction*, Mater. Sci. Semicond. Process. **37** (2015) 171.
[10] G.S. Heller, J. J. Stickler, S. Kern, A. Wold, *Antiferromagnetism in $NiTiO_3$*, J. Appl. Phys. **34** (1963) 1033.
[11] P. Van Thang, D.D. Dung, L. H. Bac, P. P. Hung, T. V. D. Ngoc, *Structural, optical, ferroelectric and magnetic properties of $NiTiO_3$ ceramic synthesized by citrate gel method*, Int. J. Nanosci. **20** (2021) 1.
[12] T. Acharya, R.N.P. Choudhary, *Structural, Ferroelectric, and electrical properties of $NiTiO_3$ ceramic*, J. Electron. Mater. **44** (2015) 271.
[13] R. Tursun, Y. Su, Q. Yu, J. Tan, *Room-temperature coexistence of electric and magnetic orders in $NiTiO_3$ and e ff ect of ethylene glycol*, Mater. Sci. Eng. B. **228** (2018) 96.
[14] P. P. Hung, D. D. Dung, N. H. Tuan, N. N. Trung, L. H. Bac, *Iron induced room temperature ferromagnetism in ilmenite $NiTiO_3$ materials*, Mater. Lett. **209** (2017) 284.
[15] M. Atif, M. Nadeem, W. Khalid, Z. Ali, *Structural, magnetic and impedance spectroscopy analysis of (0.7)$CoFe_2O_4$+(0.3)$BaTiO_3$ magnetoelectric composite*, Mater. Res. Bull. **107** (2018) 171.
[16] R. Grigalaitis, M.M. Vijatović Petrović, J.D. Bobić, A. Dzunuzovic, R. Sobiestianskas, A. Brilingas, B.D. Stojanović, J. Banys, *Dielectric and magnetic properties of BaTiO3 -NiFe2O4 multiferroic composites*, Ceram. Int. **40** (2014) 6165.
[17] K.P. Remya, R. Rajalakshmi, N. Ponpandian, *Development of BiFeO3/MnFe2O4ferrite nanocomposites with enhanced magnetic and electrical properties*, Nanoscale Adv. **2** (2020) 2968.
[18] A. Jain, Y.G. Wang, N. Wang, Y. Li and F.L. Wang, *Tuning the dielectric, ferroelectric and electromechanical properties of Ba0.83Ca0.10Sr0.07TiO_3–$MnFe_2O_4$ multiferroic composites*, Ceram. Int. 46 (2020) 7576.
[19] N. Van Dung, N. N. Hai, T. V. D. Ngoc, D. D. Tho, N. T. Nga, D. D. Dung and L.H. Bac, *Optical, ferroelectric, and magnetic properties of $NiTiO_3$–$CoFe_2O_4$ composites prepared by one-step sol–gel method*, J. Mater. Sci. Mater. Electron. **33** (2022) 18910.
[20] W. Cai, C. Fu, J. Gao, H. Chen, *Effects of grain size on domain structure and ferroelectric properties of barium zirconate titanate ceramics*, J. Alloys Compd. **480** (2009) 870.
[21] M.S. Alkathy, A. Hezam, K.S.D. Manoja, J. Wang, C. Cheng, K. Byrappa and K. C. J. Raju, *Effect of sintering temperature on structural, electrical, and ferroelectric properties of lanthanum and sodium co-substituted barium titanate ceramics*, J. Alloys Compd. **762** (2018) 49.
[22] H. Cheng, W. Zhou, H. Du, F. Luo and D. Zhu, *Effects of dwell time during sintering on electrical properties of 0.98($K_{0.5}Na_{0.5}$)NbO_3–0.02$LaFeO_3$ ceramics*, Trans. Nonferrous Met. Soc. China. **23** (2013) 2984.
[23] Y. Li, Y. Guo, Q. Zheng, K.H. Lam, W. Zhou, Y. Wan, D. Lin, *Enhancement in multiferroic and piezoelectric properties of BiFeO3-BaTiO3-Bi0.5Na0.5TiO3 lead-free ceramics with MnO_2 addition by optimizing sintering temperature and dwell time*, Mater. Res. Bull. **68** (2015) 92.